NEUROSCIENCE
RESEARCH ARTICLE

Camila Carignano et al. / Neuroscience 410 (2019) 202–216

Inner Hair Cell and Neuron Degeneration Contribute to Hearing Loss in a DFNA2-Like Mouse Model

Camila Carignano,[a1] Esteban Pablo Barila,[a1] Ezequiel Ignacio Rías,[ab] Leonardo Dionisio,[ab] Eugenio Aztiria[ab] and Guillermo Spitzmaul[ab]*

[a]*Instituto de Investigaciones Bioquímicas de Bahía Blanca (INIBIBB)–Consejo Nacional de Investigaciones Científicas y Técnicas (CONICET)–Universidad Nacional del Sur (UNS), Camino La Carrindanga Km 7, B8000FWB, Bahía Blanca, Argentina.*

[b]*Departamento de Biología, Bioquímica y Farmacia (BByF)–UNS, San Juan 670, 8000 Bahía Blanca, Argentina.*

Abstract—DFNA2 is a progressive deafness caused by mutations in the voltage-activated potassium channel KCNQ4. Hearing loss develops with age from a mild increase in the hearing threshold to profound deafness. Studies using transgenic mice for *Kcnq4* expressed in a mixed background demonstrated the implication of outer hair cells at the initial phase. However, it could not explain the last phase mechanisms of the disease. Genetic backgrounds are known to influence disease expressivity. To unmask the cause of profound deafness phenotype, we backcrossed the *Kcnq4* knock-out allele to the inbred strain C3H/HeJ and investigated inner and outer hair cell and spiral ganglion neuron degeneration across the lifespan. In addition to the already reported outer hair cell death, the C3H/HeJ strain also exhibited inner hair cell and spiral ganglion neuron death. We tracked the spatiotemporal survival of cochlear cells by plotting cytocochleograms and neuronal counts at different ages. Cell loss progressed from basal to apical turns with age. Interestingly, the time-course of cell degeneration was different for each cell-type. While for outer hair cells it was already present by week 3, inner hair cell and neuronal loss started 30 weeks later. We also established that outer hair cell loss kinetics slowed down from basal to apical regions correlating with KCNQ4 expression pattern determined in wild-type mice. Our findings indicate that KCNQ4 plays differential roles in each cochlear cell-type impacting in their survival ability. Inner hair cell and spiral ganglion neuron death generates severe hearing loss that could be associated with the last phase of DFNA2.

Key words: DFNA2, hearing loss, KCNQ4 channel, hair cells, spiral ganglion neurons.

INTRODUCTION

Potassium circulation is essential for signal transduction in the hearing process (Hibino and Kurachi, 2006; Zdebik et al., 2009), which starts with the opening of mechanosensitive cation channels placed at the tips of hair cells (Kurima et al., 2015; Pan et al., 2018). Specialized epithelium on the stria vascularis produces potassium-enriched endolymph that fills in the scala media. To maintain cell homeostasis, once potassium enters hair cells (HCs), it must return to the stria vascularis by exiting HCs and then moving through supporting cells of the organ of Corti (OC). This potassium circulation ensures that the physiological processes of hearing can take place (Hibino and Kurachi, 2006; Mistrik and Ashmore, 2009). Alterations in any of the steps involved in this circulation process can generate different kinds of hearing loss (Van Laer et al., 2006; Lang et al., 2007). KCNQ4 is the main K^+ channel involved in potassium extrusion from outer hair cells (OHCs). It is a voltage-activated channel localized at the basal pole of OHCs, generating the $I_{K,n}$ current (Kharkovets et al., 2000; Kharkovets et al., 2006; Holt et al., 2007). Its function is essential for cell survival. Mutations in KCNQ4 cause disruptions on potassium recycling and its consequences are displayed in the DFNA2 hearing loss (HL) (Kharkovets et al., 2006). This is a slow progressive deafness characterized by having two phases. The first one starts at around 15–20-year-old exhibiting a mild to moderate HL at high-frequency sounds that progresses over time to middle frequencies (Dominguez and Dodson, 2012). Hearing threshold increases 20 to 60 dB which correlates with a progressive loss of the amplificatory function exerted by OHCs (Nie,

*Corresponding author at: INIBIBB-CONICET/UNS, Camino La Carrindanga Km 7, 8000 Bahía Blanca, Argentina.
E-mail address: gspitz@inibibb-conicet.gob.ar (Guillermo Spitzmaul).
[1] These authors contributed equally to the work.
Abbreviations: OC, organ of Corti; CNS, central nervous system; HCs, hair cells; OHC, outer hair cell; IHC, inner hair cell; SGN, spiral ganglion neuron; WT, wild-type; KO, knock-out; KI, knock-in; *Kcnq4*$^{+/+}$, KCNQ4 WT mice; *Kcnq4*$^{-/-}$, KCNQ4 KO mice; HL, hearing loss; W, postnatal week-old; ARHL, age-related hearing loss; NIHL, noise-induced hearing loss; MFI, mean fluorescence intensity; SEM, scanning electron microscopy; S, 5%-length segment; K^+, potassium ion.

https://doi.org/10.1016/j.neuroscience.2019.05.012
0306-4522/

2008). The second phase is characterized by the progression of HL to a severe impairment by the age of 65–70 (De Leenheer et al., 2002). At this stage, the hearing threshold increases further beyond 70–80 dB affecting most frequencies which cannot be explained by OHC dysfunction alone (Dominguez and Dodson, 2012). Therefore, other mechanisms must be contributing to the pathology progression. Patients with this condition are heterozygous for the affected *Kcnq4* allele which bears a point mutation with a dominant-negative effect on the tetrameric channel (Kubisch et al., 1999; Dominguez and Dodson, 2012). KCNQ4 channel is not only located in OHCs, but also in inner hair cells (IHCs) and some neurons from central nervous system (CNS) nuclei of the brainstem belonging most of them to the auditory pathway (Beisel et al., 2000; Kharkovets et al., 2000; Oliver et al., 2003; Beisel et al., 2005). For these reasons, it is believed that IHCs and neurons could also participate in the progression of HL (Dominguez and Dodson, 2012). Two mouse models have been generated to analyze KCNQ4 channel contribution to the hearing process. One of them mimics DFNA2 by incorporating the equivalent human mutation G285S in one allele (*Kcnq4*$^{+/dn}$ mouse) whereas the other one carries a KO allele in both copies of *Kcnq4* gene (*Kcnq4*$^{-/-}$ mouse) (Kharkovets et al., 2006). The rate of HL in KCNQ4 transgenic animals depends on the amount of the remaining $I_{K,n}$ current, namely: a) total absence of this current (i.e. *Kcnq4*$^{-/-}$ or *Kcnq4*$^{dn/dn}$) generates rapid deafness progression correlated with an OHC loss in *Kcnq4*$^{-/-}$, b) a reduction to 1/16 of the wild-type (WT) current present in the *Kcnq4*$^{+/dn}$ is enough to delay hearing loss and OHC death for several months compared to the previous, and c) an $I_{K,n}$ current reduction of 50% does not affect cell function at all (*Kcnq4*$^{+/-}$).

Many years have passed since the molecular cause of DFNA2 was discovered (Kubisch et al., 1999). However, neither the molecular events gated by the KCNQ4 misfunction nor the role of IHCs and neurons on disease progression is fully understood. Research on DFNA2 echoes into the physiology of normal hearing and the comprehension of several hearing pathologies like age-related hearing loss (ARHL) and noise-induced hearing loss (NIHL) that share alterations in potassium circulation (Fransen et al., 2003; Van Laer et al., 2006; Dominguez and Dodson, 2012; Wong and Ryan, 2015).

Then, in order to understand the contribution of KCNQ4 to potassium homeostasis in the OC we used a KCNQ4 knockout (KO) mouse that resembles many of the characteristics observed in DFNA2 disease, although with a faster time course (DFNA2-like). Remarkably we found that in the absence of KCNQ4, not only OHCs are affected but also IHCs and SGNs. The time-course of cell death is differentially developed for each cell type, suggesting distinct roles of KCNQ4 in these cell types. Our results shed light on the mechanisms that would participate in the progression of DFNA2 deafness.

EXPERIMENTAL PROCEDURES

Animals

C3H/HeJ transgenic mice, lacking the expression of the KCNQ4 protein (*Kcnq4*$^{-/-}$), due to a deletion spanning exon 6 to exon 8, were used (Kharkovets et al., 2006; Spitzmaul et al., 2013). WT C3H/HeJ litters and C57BL/6 mice were used as controls (*Kcnq4*$^{+/+}$) and for inter-strain comparison, respectively. Mice from both sexes were employed in all experiments indistinctly. Age ranges were: a) young mice: 3, 4, 6, 8 and 10 postnatal week-old (W); b) middle-aged adult mice: 40 W, 52 W and 58 W. The experimental protocol followed in this study was approved by the Council for Care and Use of Experimental Animals (CICUAE, protocol no. 083/2016) of the Universidad Nacional del Sur (UNS), whose requirements are strictly based on the European Parliament and Council of the European Union directives (2010/63/EU).

Tissue preparation

Mice ranging from 3 W to 58 W were euthanized by CO_2 exposure and inner ears were promptly removed from temporal bones. In order to monitor hair cell and spiral ganglion neuron degeneration, cochleae were studied by immunofluorescence using two different approaches i) mounted as a whole or, ii) in thin tissue sections. Both started with tissue fixation by overnight submersion in 4% paraformaldehyde, washed with PBS, and decalcified using 8–10% EDTA in PBS for up to 5 days depending on animal age, on a rocking shaker at 4 °C.

Whole-mount cochlear preparations

The organ of Corti from decalcified cochleae was obtained following a protocol similar to that described in Akil and Lustig, 2013 and Montgomery and Cox, 2016 (Akil and Lustig, 2013; Montgomery and Cox, 2016). This method consists in splitting the whole cochlear length into three longitudinal segments: basal, middle and apical turns using fine scissors. Then, the vestibular system, spiral ligament, modiolus and tectorial membrane were removed and the organ of Corti was isolated. Finally, the hook was cut off from the rest of the basal segment.

Modiolar sections

Whole inner ears were processed according to Spitzmaul et al., 2013 and Barclay et al., 2011 (Barclay et al., 2011; Spitzmaul et al., 2013). Briefly, after decalcification, inner ears were cryoprotected in 15% sucrose for 4 h, then in 30% sucrose overnight followed by OCT embedding. 10-µm-thick sections, longitudinal to the modiolus, were obtained using a cryostat (Leica CM 1860) and preserved at −20 °C until processed.

Immunofluorescence in whole-mount cochlear preparations

Cochlear turns were postfixed in 4% PFA during 30 min, washed three times in PBS and incubated for 2 h in blocking solution (2% BSA, 0.5% Nonidet P-40 in PBS). Primary antibodies were incubated for 48 h in carrier solution (PBS containing 1% BSA, and 0.25% Nonidet P-40). Subsequently, tissue was rinsed three times in PBS. Secondary antibodies, diluted in the carrier solution, were incubated for 2 h at room temperature. After that, samples were washed three times in

PBS. Finally, cochlear turns were mounted unflattened in Fluoromount-G (Southern Biotech). The following primary antibodies were used: rabbit anti-KCNQ4 (K4C, 1:200; generously provided by Dr. T. Jentsch, Forschungsinstitut für Molekulare Pharmakologie, Berlin, Germany), goat anti-prestin (1:200, cat#sc-22,692, Santa Cruz Biotechnology), rabbit anti-myosin VIIa (1:200, cat#25-6790, Proteus Biosciences). The following fluorescently-labeled secondary antibodies were obtained from Molecular Probes and used diluted (1:500): donkey anti-rabbit 555 (cat#A-31572) and donkey anti-goat 488 (cat#A-11055). Nuclei were stained with DAPI (1:1000).

Hair cell counting and cytocochleogram plotting

Labeled cells on whole-mount cochleae were imaged using an epifluorescence microscope (Nikon Eclipse E-600) coupled to a CCD camera (Nikon K2E Apogee) and a laser spectral confocal microscope (Leica TCS SP2). Pictures were analyzed using the Image J software and cell counting was carried out manually. HCs were identified based on their tissue localization in the OC. For OHCs, row 1 was considered as the innermost cell line followed by row 2 corresponding to the middle line of cells and row 3 to the outermost cell line. Cellular degeneration was evaluated on a cytocochleogram (four to five animals for each age and genotype). A cytocochleogram is basically a cartographical approach used for determining HC number and distribution along the entire cochlear length (Viberg and Canlon, 2004; Muller et al., 2005; Boyce et al., 2010; Sanz et al., 2015). It is constructed by plotting the number of OHCs or IHCs versus the relative distance to the apex. In order to normalize the OC's length, cells were counted separately in 20 segments (S), each of them spanning 5% of the total cochlear length, which was considered the whole (100%) distance. Each S was numbered according to the spanning percentage of the total length, starting from the apex (e.g. from 0% to 5% = S5), to the basal end (S100). Apical, middle and basal turns were defined as those spanning S5 to S35, S40 to S70 and S75 to S100, respectively.

Cell loss rate estimation

The dynamic of cell loss was calculated plotting the average number of living cells in each segment vs. mice age on a logarithmic scale. Data were fitted through the SigmaPlot 12.0 software (Systat Software Inc.) using a sigmoidal equation as follows:

$$\mathrm{N}_{OHC} = OHC_{max} \cdot \frac{(\mathrm{Age})^{nH}}{\left[\mathrm{CD50}^{nH} + (\mathrm{Age})^{nH}\right]}$$

where N_{OHC} represents the number of cells at each age (in weeks), OHC_{max} is the initial OHC number, CD_{50} is the age where 50% cell death was achieved, and nH estimates cell death rate.

Immunofluorescence on cochlear sections

Slide-mounted tissue sections were post fixed with 2% PFA for 20 min, washed with PBS and blocked in the same buffer as described in section 2.3. Slice sections were incubated overnight with a primary antibody rabbit anti-beta III Tubulin (tuj1, Covance #mrb-435p) diluted 1:1000 in the carrier solution. A fluorescently-labeled goat anti-rabbit 488 (Molecular Probes, cat#A-11034) was used as secondary antibody, which was incubated during 1 h.

Spiral ganglion neuron density measurements

10-μm-thick cochlear longitudinal slices, comprising the whole extension of the modiolus, were chosen to perform SGN assessment. Using a 20× magnification objective, fluorescent images were taken for each of the ganglion individual portions (i.e.: basal, medial and apical). Images were processed with Image J by demarcating their area and taking into account the bound space of bone surrounding the ganglia and the extent of beta III tubulin staining. Using the cell counter extension of this software, individual cells were counted manually, and their density was calculated by dividing the number of SGNs over the area in square micrometers covered by the ganglion. Results were plotted for each portion of the ganglion versus the age, in weeks, for each mouse genotype.

KCNQ4 signal intensity

The expression pattern of the KCNQ4 channel in OHCs was analyzed on whole-mount cochlear preparations from WT mice at different ages. To do so, the organ of Corti was divided into 3 segments, as explained above. To quantify the differences, we measured the mean fluorescence intensity (MFI) of each cell in confocal images using Image J software. We measured the intensity of at least 20 OHCs for each row in the central area of each turn. Background noise was calculated from averaging the signal of five to six representative areas where no immunofluorescence was apparent. Specific signal was calculated by subtracting the averaged background value from that of each immunopositive cell.

RNA extraction and qPCR

Cochlear RNA was extracted from 3-week-old mice. For each experiment, samples from three to four mice were pooled. In brief, immediately after cochlear excision, tissue was immersed in an RNA preservation buffer and then, the vestibular region was removed to keep only the cochlea. Using a scalpel, the cochlea was cut between the first and second turn, in order to obtain a bottom piece containing the basal turn and another one containing the middle and apical turns. RNA was extracted using the TransZol reagent (TransGen Biotech, ET101-01) in combination with the Direct-Zol RNA mini prep kit (Zymo Research, R2052), essentially as indicated in Patil et al. (Vikhe Patil et al., 2015). cDNA was produced from 500 ng total RNA with EasyScript Reverse Transcriptase (TransGen Biotech Cat #AE101) using anchored oligo (dT)s following manufacturer's indications.

Quantitative PCR (qPCR) was carried out using the cDNA generated previously employing the SensiFAST SYBR mix No-Rox Kit (Bioline) in a Rotor-Gene 6000 real-time PCR cycler (Corbett Research). Primers for the *KCNQ4* gene were: 5′-TATGGTGACAAGACGCCACAT-3′ (forward) and 5′-GGCAGAAGCACTTTGAGAAGC-3′ (reverse) while for the reference genes were as follows: HPRT 5′-GTTCT TTGCTGACCTGCTGGA-3′ (fwd) and 5′-AATGATCAGT CAACGGGGGA-3′ (rev); GAPDH 5′-GAGAAACCTGCCAA GTATGATGAC-3′ (fwd) and 5′-CCCACTCTTCCACCTTC GAT-3′ (rev). Data analysis was done applying the ΔΔCt method (Livak and Schmittgen, 2001) to obtain relative mRNA expression.

Scanning electron microscopy (SEM)

Basal cochlear segments were dissected from *Kcnq4*$^{+/+}$ and *Kcnq4*$^{-/-}$ at 4 W and 6 W. Cochleae were fixed using 2.5% glutaraldehyde for 2 h and then, decalcified as mentioned previously. Samples were dehydrated with ethanol and a critical point drier was applied. Finally, tissues were imaged with a LEO-EVO 40 XVP-EDS Oxford X-Max 50 scanning electron microscope provided by the Microscopy Facility from Centro Científico Tecnológico–Bahía Blanca (CCT-BB) / CONICET.

Statistical analysis

All data and results were confirmed through at least, three independent experiments. Shown values represent the means ± SEM. Significant differences were identified using, i) Student's t-test for experiments shown in Figs. 1C, 3B (for comparison between WT and KO mice at 3 W), Fig. 5B (for comparison between WT and KO mice at 10 W) and Fig. 7B; ii) one-way ANOVA in Figs. 3B, 4A, 5B and 7D; iii) two-way ANOVA for results shown in Fig. 6C. Bonferroni or Tukey's Multiple Comparison Tests were used when ANOVA detected differences. Statistical analyses were performed using Excel and SigmaPlot 12.0 Software. Statistical significance is represented with (*) when $p < 0.050$; (**) when $p < 0.010$ and (***) when $p < 0.001$.

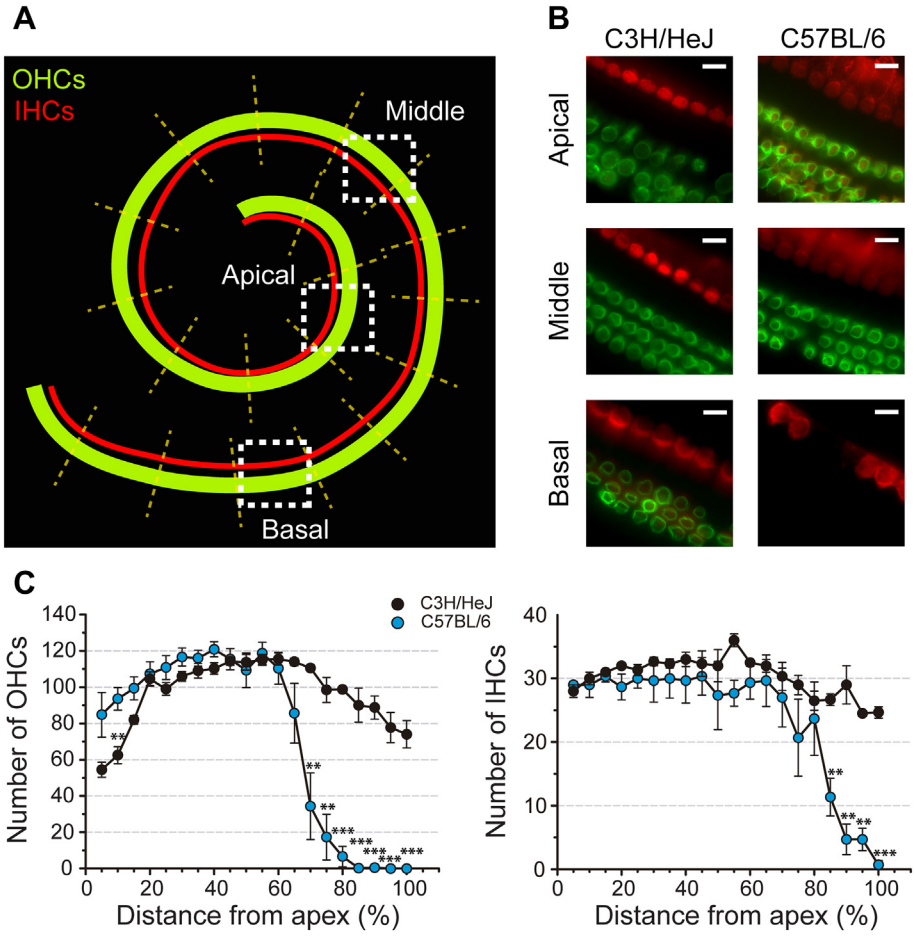

Fig. 1. Hair cell survival comparison between C3H/HeJ and C57BL/6 middle-aged adult mice. (A) Schematic representation of a mouse Organ of Corti showing its whole extension. OHC (green) and IHC (red) cochlear localization is depicted. Dashed white squares delimit the areas represented on B panel. Dashed yellow lines indicate segments spanning 5% of the entire cochlear length (S) that were used to build cytocochleograms. Each S was referred relative to the apex. **(B)** Representative pictures showing hair cell presence in apical, middle and basal turns in C3H/HeJ (left) and C57BL/6 (right) mice at 52 W. IHCs and OHCs were labeled with anti-prestin (green) and anti-myosin VIIa (red) antibodies, respectively. Scale bar: 10 μm. **(C)** Comparison of hair cell degeneration between C3H/HeJ and C57BL/6 mice at 52 W. Cytocochleograms showing OHC (left) and IHC (right) counts for each S in C3H/HeJ (black) and C57BL/6 (light blue) strains. Data are represented as means ± SEM (n = 3–4 animals). Comparisons were performed using Student's t-test between cell number from both strains at each S. Asterisks indicate statistical differences: $p < 0.050$ (*), $p < 0.010$ (**) and $p < 0.001$ (***).

RESULTS

Effect of genetic background on cochlear cell survival

Genetic backgrounds are well-known to influence disease phenotype (Doetschman, 2009). Previous studies with *Kcnq4* KO allele performed on a mixed background between C57BL/6 and 129/SV mouse strains displayed only OHC disappearance, resembling an accelerated initial phase of DFNA2 (Kharkovets et al., 2006). To better reproduce a DFNA2-like phenotype including early and late phases but in a shorter time frame, we expressed the *Kcnq4* KO allele in the C3H/HeJ strain. In this last, hearing function is well-preserved beyond 1-year-old with a low

incidence of ARHL (Trune et al., 1996). For this reason, it is a suitable background to evaluate progressive hearing loss in aged mice due to external factors. Thus, we first analyzed cell survival in 52 W WT C3H/HeJ mouse strain to determine normal hair cell loss. Then we contrasted these data with those of age-matched C57BL/6 mouse strain, a known model for ARHL (Davis et al., 2001). We used a standard procedure based on cytocochleographic analysis, which related cell counts with cochlear segments (see Experimental Procedures). OHCs were identified using an anti-prestin antibody and IHCs by anti-Myosin VIIa antibody (Kharkovets et al., 2006; Dallos, 2008; Spitzmaul et al., 2013). Fig. 1A (left) depicts a schematic division of the cochlea that was performed for the whole-mount of the organ OC. Traversed yellow dashed lines indicate the boundaries of the 5%-length segments (S) in which the entire cochlea was divided and where hair cells were counted (see Experimental Procedures). Both strains showed robust signals for OHCs (green) and IHCs (red) in the three cochlear turns. While C3H/HeJ showed the normal pattern of HC distribution with almost no gaps, C57BL/6 exhibited missing cells in basal and middle turns for both HC types (Fig. 1B). We plotted cytocochleograms to show cell survival and distribution along the cochlea at each S for both strains in 52 W animals (Fig. 1C). We chose this age because ARHL is already consolidated in C57BL/6 strain (Erway et al., 1993). Comparing each segment between strains we found that C3H/HeJ mice displayed a statistically significant higher number of OHCs than C57BL/6 mice from S70 forwards ($p < 0.010$ for S70 and S75 and $p < 0.001$ for S80, S85, S90, S95 and S100, Student's t-test). We made a similar observation for IHCs, where we obtained higher cell counts statistically significant in the basal turn of C3H/HeJ than that of C57BL/6 mice. Significant differences were observed at S85, S90 and S95 ($p < 0.010$, Student's t-test) and S100 ($p < 0.001$, Student's t-test) (Fig. 1C, right). Thus, our results indicate a high proportion of HC survival in C3H/HeJ strain, enabling us to analyze the role of KCNQ4 channel in this process for at least up to 1 year of age.

Effect of KCNQ4 deletion on cochlear cell survival in middle-aged mice

To have an overview of the impact of KCNQ4 channel absence on cell survival, we determined the number of OHCs, IHCs and SGNs in the three cochlear turns at 58 W WT and *Kcnq4*$^{-/-}$ mice (Fig. 2). *Kcnq4*$^{+/+}$ cochlea showed the presence of all three rows of OHCs in the three turns with occasional missing cells in apical or basal turns (Fig. 2A), as described in Fig. 1. No loss was observed either for IHCs or SGNs counts, whose average values were 32.3 ± 3.0 cells/turn for IHCs and 36.0 ± 1.9 cells/0.01 mm^2 for SGNs (Fig. 2A, left). In contrast, we found a differential decrease for each cell type in *Kcnq4*$^{-/-}$ mice (Fig. 2A, right). To better understand the spatial progression of cell death, we calculated the cell survival ratio between KO and WT animals in each cochlear turn. We observed a drastic decrease of OHCs, from 60% in the apical turn to a complete absence in the basal turn (Fig. 2B, green bars). For IHC, we observed a mild cell loss in apical and middle turns, but a severe cell loss in basal turn (~85%) (Fig. 2B, red bars). For SGNs apical and basal turns were the most affected, with a 50% and a 30% of cell survival, respectively, while the middle turn did not exhibit cell loss at all (Fig. 2B, blue bars).

OHC loss along the Organ of Corti in *Kcnq4*$^{-/-}$ mice

KCNQ4 channel absence impairs K^+ extrusion from OHCs which would disturb K^+ recycling in the inner ear, leading to OHC death and tissue degeneration (Kharkovets et al., 2006). We monitored cell survival in cochlear whole-mount preparations from WT and *Kcnq4*$^{-/-}$ mice from 3 W to 58 W. First, we analyzed tissue length to avoid miscalculation of cell counts and found that was similar for both genotypes. Average length values were 5497 ± 190 µm (n = 24) and 5465 ± 168 µm (n = 26) for *Kcnq4*$^{+/+}$ and *Kcnq4*$^{-/-}$ mice, respectively ($p > 0.050$, Student's t-test).

In order to evaluate the spatial and temporal OHC loss exhibited by the *Kcnq4*$^{-/-}$ mouse, we performed cytocochleographic analysis to both mouse genotypes at different ages. While in WT animals the consecutive three row-pattern of OHCs remained almost constant with age, we observed missing OHCs in several rows, altering the regular pattern in *Kcnq4*$^{-/-}$ mice (Fig. 3A, see also Fig. 2A, OHC panel).

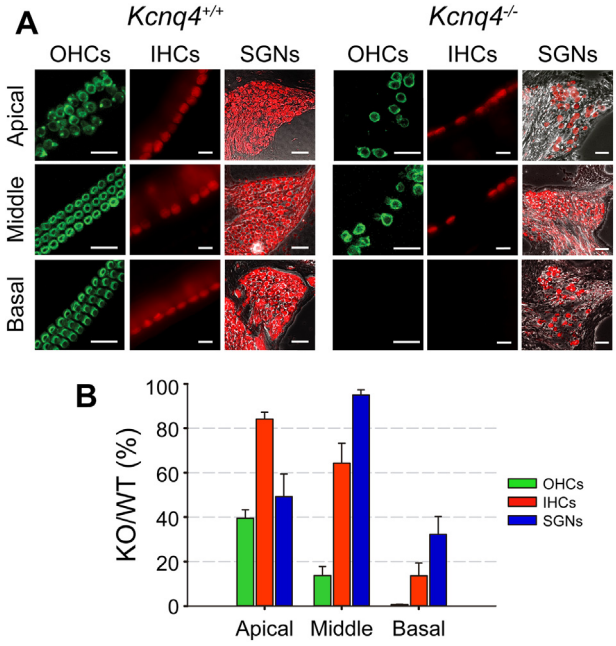

Fig. 2. Differential impact of KCNQ4 channel absence on cochlear cell survival. (A) Pictures from apical, middle and basal turns showing OHCs, IHCs and SGNs in *Kcnq4*$^{+/+}$ and *Kcnq4*$^{-/-}$ mice at 58 W. OHCs and IHCs were labeled as described in Fig. 1. SGNs were identified with anti-β-III tubulin (red). Scale bars for OHCs, 20 µm; IHCs, 10 µm and SGNs, 50 µm. **(B)** Bar plot depicting normalized cell survival. Cell survival ratios for OHCs (green), IHCs (red) and SGNs (blue) in the three cochlear turns at 58 W are shown as percentage. Ratios were calculated as the average cell number of *Kcnq4*$^{-/-}$/*Kcnq4*$^{+/+}$ mice (KO/WT) for each turn. Data are represented as means ± SEM (n = 3–7).

Indeed, cell disappearance increased with age (Fig. 3A, right). To determine control cell survival values for each segment in young and middle-aged animals, we constructed cytocochleograms for WT mice at different ages. When compared to 3 W mice, an age where the auditory system is mature (Bulankina and Moser, 2012), our data showed a mild decrease in cell survival for middle-aged animals in the apical turn (S5 and S10: $p < 0.050$ for 40 W, 52 W and 58 W; S15: $p < 0.050$ for 52 W, one-way ANOVA, post hoc Bonferroni test). From S20 forwards, the number of OHCs in every segment did not change with age ($p > 0.050$ for each segment, one-way ANOVA) (Fig. 3B, left).

On the other hand, OHC survival drastically changed in *Kcnq4*$^{-/-}$ animals (Fig. 3B). At the youngest studied age (3 W), OHC counts at each segment were similar than those in *Kcnq4*$^{+/+}$ animals until S80 ($p > 0.050$ for each segment, Student's t-test). From S85 to S100, cell number progressively decreased, exhibiting ~85% OHC loss at the cochlear hook ($p < 0.050$ for each segment, Student's t-test) (Fig. 3B, right). In consequence, cell loss is already present even in young KO animals. Compared to 3 W *Kcnq4*$^{-/-}$ animals, as mice grew old, the number of OHCs decreased progressively in every segment, across the entire cochlear length (Fig. 3B, right). For each segment, we analyzed the decrease in cell counts with age. While we did not find significant differences between 3 W and 4 W (Table 1), cell survival gradually decreased becoming significant from basal to apical segments with age (one-way ANOVA, post hoc Bonferroni test) (Table 1, Fig. 3B). Middle-aged adult *Kncq4*$^{-/-}$ mice exhibited a complete absence of OHCs in basal segments from S80 forwards. Middle-to-apical segments were less sensitive to the loss of the KCNQ4 protein showing a 20–40% of remaining OHCs (Fig. 3B, right).

In order to evaluate the kinetics of OHC loss in cochlear turns, we analyzed the rate of cell loss at every S by plotting the number of OHCs against mouse age (Fig. 3C). While in *Kcnq4*$^{+/+}$ mice the number of OHCs remained constant over time (Fig. 3C, open symbols), it decayed in *Kcnq4*$^{-/-}$ animals (Fig. 3C, closed symbols). The loss of OHCs was slow at the youngest ages but increased drastically in the following weeks until cells degenerated completely at the oldest ages. Most apical segments (S5 and S10, not shown) did not follow this pattern, probably due to an overestimation of cell death resulting from the slight age-dependent HL observed also in *Kcnq4*$^{+/+}$ mice (see Fig. 3B). To describe the

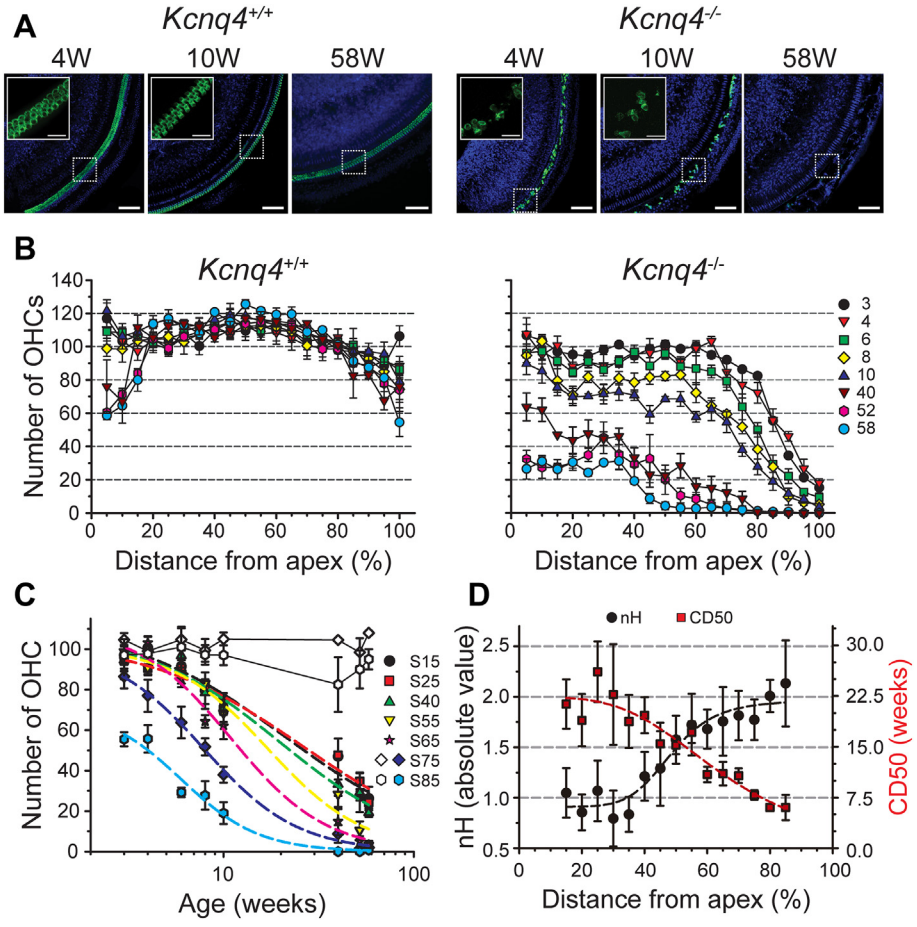

Fig. 3. Spatiotemporal analysis of OHC loss in *Kcnq4*$^{-/-}$ mice. (A) Representative pictures of OHCs from *Kcnq4*$^{+/+}$ (left) and *Kcnq4*$^{-/-}$ (right) mouse cochleae. Whole-mount sections show OHCs from basal turns at 4 W, 10 W and 58 W labeled with anti-prestin (green) antibody. Scale bar: 75 µm. Nuclei were stained with DAPI (blue). Insets show a higher magnification of the area delimited by the corresponding dashed white lines. Scale bar: 20 µm. Insets corresponding to 58 W are shown in Fig. 2A. **(B)** OHC cytocochleograms of *Kcnq4*$^{+/+}$ (left) and *Kcnq4*$^{-/-}$ (right) mice across 3 W to 58 W range. Values represent the mean number of OHC in each S and age ± SEM (n = 3–5). Symbols indicate mouse age (W) and correspond to: 3 W: black circle, 4 W red inverted triangle, 6 W: green square, 8 W: yellow diamond, 10 W: blue triangle, 40 W: brown inverted triangle, 52 W pink hexagon, 58 W: light blue circle. **(C)** Assessment of OHC loss rates at each segment for *Kcnq4*$^{-/-}$ mice. OHC mean counts were plotted at the indicated S vs. age (taken from panel B). Data were fitted using a sigmoidal equation (dashed lines) (see Experimental Procedures). Symbols for the different S are: S15: black circle, S25: red square, S40: green triangle, S55: inverted yellow triangle, S65: pink star, S75: blue diamond and S85: light blue hexagon. Open diamond and hexagon correspond to WT S75 and S85, respectively. Data are represented as means ± SEM (n = 3–5) **(D)** Kinetic parameters for the sigmoidal equation corresponding to each segment. nH (left axis) and CD50 (right axis) were plotted. Symbols correspond to: nH: black circles, CD50: red squares. Data are represented as means ± SEM (n = 3–5).

kinetics of cell loss we used a sigmoidal equation to fit our temporal data for each S. Slopes for apical to middle segments (S15 to S40) were less pronounced than those observed in basal segments (Fig. 3C). In order to visualize the behavior of OHC loss rates, we plotted nH and the CD50s obtained from fitted curves for *Kcnq4*$^{-/-}$ mice at each cochlear S (Fig. 3D). nH progressively increased from apical (nH ~0.9) to basal (nH ~2.0) segments in a sigmoidal shape. Conversely, we observed that CD50 decreased with increasing distance from the apex, from an initial value of around 22 weeks (S15) to a value of 7 weeks at S85 (Fig. 3D). Changes in coefficient values indicate that the kinetics of OHC loss is not homogenous along cochlear segments, speeding up from apical to basal turns. For the same age, OHC number will decrease in apical segments proportionally to $\frac{(\text{Age})^{-1}}{[22^{-1}+(\text{Age})^{-1}]}$ while in basal segments it will be $\frac{(\text{Age})^{-2}}{[7^{-2}+(\text{Age})^{-2}]}$.

Alteration of OHC row architecture and stereocilia structure in *Kcnq4*$^{-/-}$ mice

To get insights into OHC degeneration, we analyzed the time-course pattern of OHC survival in each individual row. Cochleographic studies were carried out in the S20–S60 range for young animals (6 W to 10 W) since OHC degeneration from these cochlear regions is ongoing within this timeframe, but cell row architecture is still well preserved (Fig. 4A, left). In *Kcnq4*$^{+/+}$ mice, we did not observe differences among OHC counts for each row, exhibiting an average value of ~37 cells/row for each segment ($p > 0.050$ one-way ANOVA) (Fig. 4A). In agreement with the results shown above, the OHC number for each row decreased with age in *Kcnq4*$^{-/-}$ animals. However, OHC loss was not equivalent among the three rows (Fig. 4A). Indeed, the highest decrease was observed for the central row 2. At 6 W, only two segments of row 2 showed statistically significant differences with respect to the internal row 1 and the external row 3: S25 and S50 ($p < 0.050$ and $p < 0.010$, respectively; one-way ANOVA, post hoc Tukey test). The rest of the segments in row 2 exhibited lower cell counts than row 1 and 3, which did not reach statistical significance, suggesting a trend towards higher cell death rate (Fig. 4A). At 8 W and 10 W, differences between row 2 and the others became more evident. Indeed, at these ages, five to six segments out of nine in row 2 showed significant differences (p-values in Fig. 4A legend; one-way ANOVA, post hoc Tukey test) (Fig. 4A).

Due to the differential cell loss among rows and to better understand the process of tissue degeneration, we studied apical surface by SEM (Fig. 4B). As expected, WT mice inspection at 4 W and 6 W showed the characteristic three-row distribution of OHCs without spaces between them (Fig. 4Ba and Bb). In addition, individual cells bared the typically polarized hair bundle structure, where the upper surface ends up with ordered and neat rows of stereocilia, arranged in a three-step staircase profile, exhibiting the characteristic W shape (Fig. 4Bc and Bd). On the other hand, basal cochlear segments of *Kcnq4*$^{-/-}$ mice, even at 4 W, showed clear alterations in tissue arrangement. The typical three-row pattern was still recognizable in some regions but not clearly defined in others (Fig. 4Be and Bf). Cell loss became apparent at this age because several hair bundles were missing and replaced by scars on the tissue surface. OHC loss was even greater at 6 W (see white arrows in Fig. 4Be and Bf), these results being in agreement with those described above (see Figs. 3 and 4A).

In addition to cell loss, hair bundle structure in the still surviving cells exhibited evident damage showing a disorganized pattern (Fig. 4Bg and Bh). Fig. 4B allowed to identify several steps of the degenerative process, starting from the tip-fusion of the three stereociliary rows (asterisk), progressing to "walls" of fused stereocilia (yellow arrowhead) in which individual ones are no longer recognizable. Occasionally, it was also possible to observe floppy stereocilia (white arrowhead). Fusion processes can span from small to big portions of the bundle. In some cases, stereocilia fusion between two different bundles could be observed. So, OHCs not only displayed cell loss but also several alterations in their apical structure. Stereocilia alterations were not observed for IHCs in this time period (not shown).

Table 1. Statistical analysis of OHC survival at different ages for representative cochlear segments (S) in *Kcnq4*$^{-/-}$ mice.

Age Comparison (W)	S5	S20	S35	S50	S65	S80	S95
3 vs. 4	ns	ns	ns	ns	ns	ns	ns
3 vs. 6	ns	ns	ns	ns	ns	ns	*
3 vs. 8	ns	ns	ns	ns	**	***	**
3 vs. 10	ns	*	**	**	***	***	***
3 v. 40	***	***	***	***	***	***	***
3 vs. 52	***	***	***	***	***	***	***
3 vs. 58	***	***	***	***	***	***	***

One-way ANOVA and post hoc Bonferroni test were performed for each segment to compare changes in cell survival with age, taking values from 3 W mice as reference. Symbols indicate the statistical differences found in each case which correspond to: ns: $p > 0.050$; *: $p < 0.050$; **: $p < 0.010$ and ***: $p < 0.001$.

Degeneration of IHCs also occurs in KCNQ4 absence

As we did for the OHC degeneration study, we used cytocochleographic analysis to evaluate IHC loss in WT and KO mice. For this we evaluated IHC survival in young and middle-aged adult animals. *Kcnq4*$^{+/+}$ mice exhibited a continuous single row of IHCs in basal turn at all tested ages (Fig. 5A, left). On the contrary, in *Kcnq4*$^{-/-}$ mice, the loss of IHCs is evident only in adult animals (Fig. 5A, right). In the analysis of *Kcnq4*$^{+/+}$, each cochlear segment showed similar IHC counts across the entire cochlear length in middle-aged mice when compared to young animals (10 W) ($p > 0.050$ for each Segment, one-way ANOVA) (Fig. 5B, left). In *Kcnq4*$^{-/-}$ 10 W mice, the number of IHC remained similar to WT values for each segment ($p > 0.050$ for each S, Student's t-test). However, middle-aged adult mice showed loss of IHCs, already present at 40 W in basal segments, progressing to middle segments in 52 W and 58 W animals (Fig. 5B, right). Compared to 10 W mice, older KO animals displayed

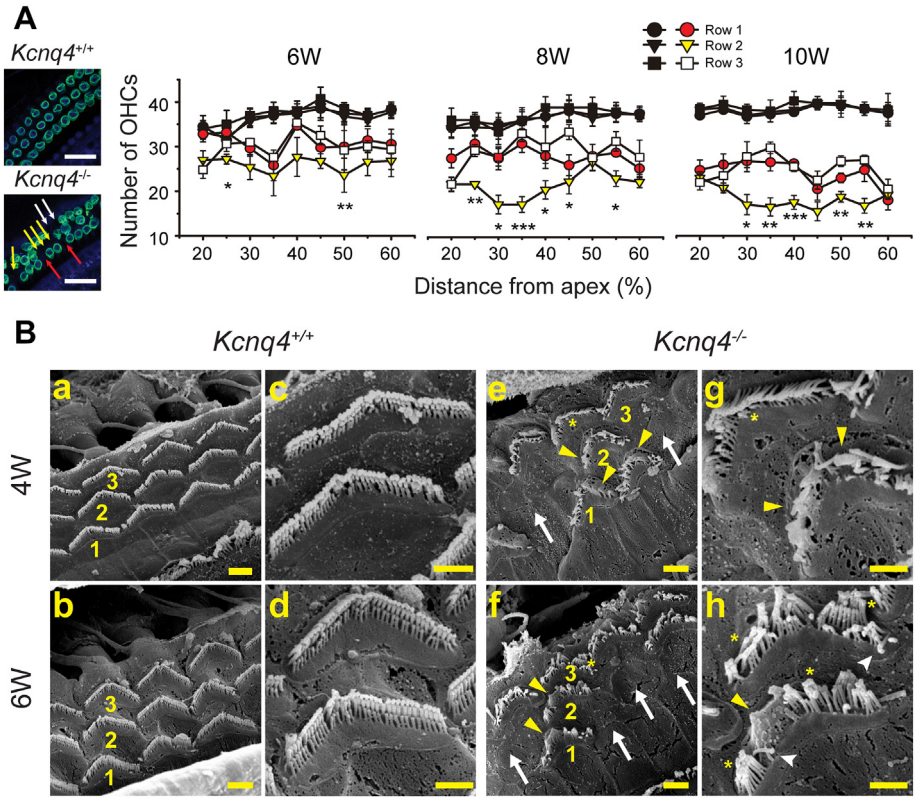

Fig. 4. Row architecture and surface ultrastructure of OHCs in young *Kcnq4*$^{-/-}$ mice. (A) OHC survival analysis for each of the three rows. The left side shows representative immunofluorescence pictures from 10 W *Kcnq4*$^{+/+}$ (upper) and *Kcnq4*$^{-/-}$ mice (lower). OHCs were labeled with anti-prestin (green) and nuclei with DAPI (blue). Arrows point out missing OHCs in row 1 (red), row 2 (yellow) and row 3 (white), in *Kcnq4*$^{-/-}$ mouse. Scale bar, 25 μm. On the right it is displayed average OHC counts for each row in WT (dark symbols) and KO (colored symbols) mice. OHCs were counted separately for row 1 (circle), row 2 (triangle) and row 3 (square) in the S20–S60 range at different ages. Data are represented as means ± SEM from 4 to 5 independent experiments. For statistical analysis, each row was compared to the other two, at each segment in both genotypes. No statistical differences were observed among rows for *Kcnq4*$^{+/+}$ animals at all ages. Asterisks indicate statistical differences between row 2 and the other two for *Kcnq4*$^{-/-}$ animals. At 6 W; S25, $p < 0.050$ (*) (row 1 vs. row 2) and S50; $p < 0.010$ (**) (row 2 vs. row 3). At 8 W, S25; $p < 0.010$ (**) (row 2 vs. row 3); S30, $p < 0.050$ (*) (row 2 vs. row 3); S35, $p < 0.001$ (***) (row 2 vs. row 3); S40, $p < 0.050$ (*) (row 2 vs. row 3); S45, $p < 0.050$ (*) (row 2 vs. row 3) and S55, $p < 0.050$ (*) (row 2 vs. row 3). At 10 W; S30, $p < 0.050$ (*) (row 2 vs. row 3); S35, $p < 0.010$ (**) (row 2 vs. row 3); S40, $p < 0.001$ (***) (row 1 vs. row 2); S50, $p < 0.010$ (**) (row 2 vs. row 3) and S55, $p < 0.010$ (**) (row 2 vs. row 3) (one-way ANOVA, post hoc Tukey test). **(B)** Apical surface analysis of hair cells by scanning electron images in WT (a–d) and KO mice (e–h). Pictures at low (a, b, e and f) and high (c, d, g and h) resolution are shown for 4 W (upper) and 6 W (lower) mice. Internal, middle and external OHC rows are indicated as 1, 2 and 3, respectively. Symbols indicate: white arrows, OHC absence; white arrowheads, floppy stereocilia; yellow asterisks, tip-fused stereocilia and yellow arrowhead indicate whole-fused structures. Scale bar: 2 μm in a, b, e and f and 1 μm in c, d, g and h.

differences in the IHC counts reaching significance from S85, S70 and S55 onwards for 40 W, 52 W and 58 W mice, respectively (p-values for each segment in Figure's legend 5B, one-way ANOVA, post hoc Bonferroni test) (Fig. 5B, right). Indeed, at S75, IHC counts became lower than 10 cells/S reaching a complete IHC loss in basal segments in 40 W to 58 W animals.

We also performed kinetic studies for IHCs. Contrary to OHCs, IHC loss is only observed from S55 onward, so we studied this range. Cell loss developed abruptly with age for each segment, exhibiting high nH values, such as 4.9, 11 and 24 for S60, S65 and S70, respectively, when fitted with a sigmoidal equation. Due to the low number of living cells in the most basal segments, we were unable to fit representative curves for S80 to S100. The kinetics of cell loss for the fitted segments developed very fast with age, progressing exclusively from basal to middle turns up to 58 W (not shown).

Spiral ganglion neurons also degenerate in *Kcnq4*$^{-/-}$ mice

We also analyzed SGN survival in mice lacking KCNQ4 channel expression on modiolar cochlear sections. Neuronal density was determined in spiral ganglia from basal, middle and apical turns at different ages (Fig. 6A, dashed lines). WT mice displayed a high number of neurons in each ganglion turn at all ages while *Kcnq4*$^{-/-}$ animals exhibited a decrease in neuron number in basal and apical ganglion turns at 58 W (Fig. 6B). Estimation of neuronal densities showed that *Kcnq4*$^{+/+}$ mice exhibited an average value of 36–39 neurons/0.01mm^2 for the three cochlear segments at 10 W. This value remained practically constant through age for the different segments ($p > 0.050$, two-way ANOVA) (Fig. 6C). On the contrary, in *Kcnq4*$^{-/-}$ animals, we determined a neuronal loss that varies differentially with ganglion localization. A clear neuronal loss was seen in basal and apical turns in KO mice older than 1 year when compared to WT animals ($p < 0.001$, two-way ANOVA, post hoc Bonferroni test) (Fig. 6C, asterisks). As the number of SGNs at 10 W in all segments of *Kcnq4*$^{-/-}$ mouse was not statistically different from that of *Kcnq4*$^{+/+}$ mouse, we used these values as reference to evaluate cell death. Neuron density gradually decreased for basal and apical turns as mice grew old, while it remained almost invariable for middle segments. Although a great variability was obtained for neuronal density estimations due to unevenness in cochlear slices, neuron counts reached statistical significance at 52 W in the basal and apical segments that increased with age ($p < 0.010$ for 52 W and $p < 0.001$ for 58 W, two-way ANOVA, post hoc Bonferroni test) (Fig. 6C, hash symbol). At 58 W, neuronal loss was larger than 50%, compared to 10 W animals in both turns (Fig. 6C). In middle segment, neurons exhibited a slight but significant decrease in neuron counts between 10 W to

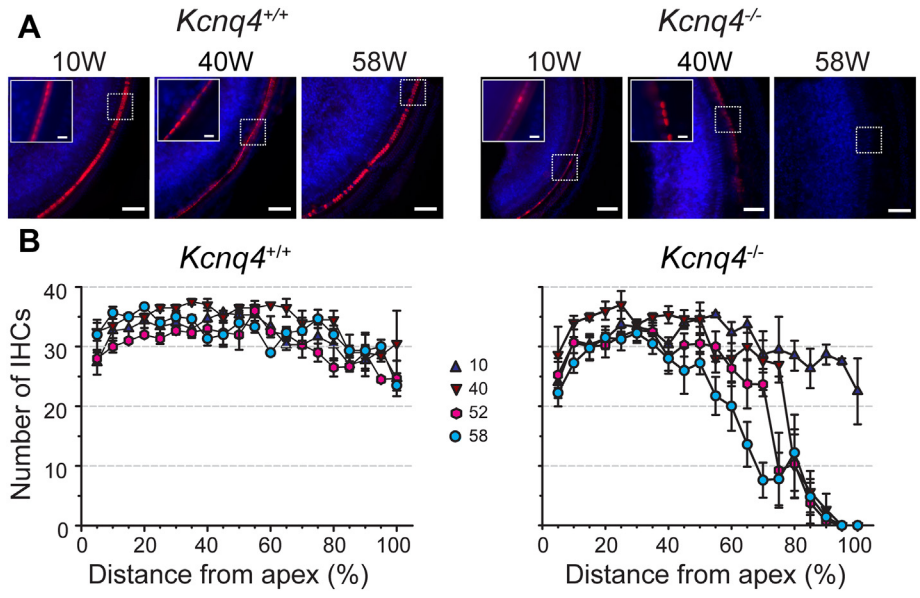

Fig. 5. Spatiotemporal analysis of IHC loss in *Kcnq4*$^{-/-}$ mice. (A) Representative pictures of WT (left) and KO (right) mice cochleae at 10, 40 and 58 W showing IHCs in basal turn. IHCs were labeled using anti-myosin VIIa (red) antibody in cochlear whole-mount preparations. Nuclei were stained with DAPI (blue). Scale bar: 50 μm. Insets show a higher magnification of the area delimited by the corresponding dashed white lines. Inset pictures for 58 W mice are shown in Fig. 2A. Scale bar: 10 μm. **(B)** IHC cytocochleograms of *Kcnq4*$^{+/+}$ (left) and *Kcnq4*$^{-/-}$ (right) mice at several ages. Values represent the mean number of IHC in each S and age ± SEM (n = 3–5). Symbols indicate mouse age (W) and correspond to 10 W: blue triangle, 40 W: brown inverted triangle, 52 W: pink hexagon, 58 W: light blue circle. For KO mice at 40 W, $p < 0.050$ at S85, $p < 0.001$ at S90, S95 and S100. For 52 W, $p < 0.050$ at S70, S75, S80 and S85; $p < 0.001$ at S90, S95 and S100. For 58 W, $p < 0.010$ at S55, S60, S65, S70, S75, S80 and S85; $p < 0.001$ at S85, S90, S95 and S100. One-way ANOVA, post hoc Bonferroni test.

40 W animals ($p < 0.010$, two-way ANOVA, post hoc Bonferroni test). However, this number did not further increase with age, indicating that SGNs were better preserved in this turn (Fig. 6C). In summary, in *Kcnq4*$^{-/-}$ mice, SGNs also degenerate but later than OHCs and timely-tuned to IHC loss.

Correlation between cell loss time-course and expression of KCNQ4 channel

To expose the differences in the time-course of IHC, OHC and SGN loss, we calculated the survival ratio between *Kcnq4*$^{-/-}$ and WT animals for each cell type at four different ages (Fig. 7A). We plotted cytocochleogram survival ratios for IHCs and OHCs, while for SGNs the representative values obtained for apical, basal and middle turns were plotted at S20, S50 and S85, respectively. While OHC loss is observed at all periods, increasing with age, IHCs started at 40 W only after S75 (Fig. 7A). SGN disappearance slightly started at basal turn in 40 W mice, increasing both basal and apical turn in older mice. A clear difference in the spatial and temporal pattern of cell loss was evident between IHCs and OHCs. For the same age, a similar cell loss proportion (e.g. 40%) is reached at S75–80 for IHCs and S10–15 for OHCs, indicating that, when IHC loss is present at the basal segment, OHC degeneration had already reached the middle to apical segments (Fig. 7A). Besides, we observed a shift in the time-course. For example, comparing the same segment (e.g. S80), IHCs reached an 80% cell loss at 40 W while the same proportion of OHCs was obtained at 10 W (Fig. 7A). Thus, there was a delay of IHC degeneration of about 30 weeks compared to OHC degeneration. SGN degeneration followed a similar time-course pattern than IHCs (Fig. 7A).

Then we analyzed KCNQ4 channel expression in C3H/HeJ WT mice. Using reverse transcription followed by qPCR, we evaluated the expression level of *Kcnq4* mRNA in basal and middle/apical cochlear turns of WT young mice. As shown in Fig. 7B, middle/apical turns exhibited around a 50% less *Kcnq4* mRNA compared to the basal turn ($p < 0.010$, Student's t-test).

The expression of the KCNQ4 protein was evaluated by MFI level measurements performed on cochlear whole-mounts. KCNQ4 signal was clearly detected in the three OHC rows while no signal was observed either for IHCs or for SGNs (Fig. 7C). The fluorescent signals from the basal, middle and apical turns were compared for young mice. Similar fluorescence intensities were detected in the three rows of OHCs for the same turn; however, it varied with the different turns (Fig. 7C). Fluorescent signal was robust in basal and middle turns, but it was weaker in cells of the apical turn. To quantify the KCNQ4 expression level, we measured MFI levels in young animals. As shown in Fig. 7D, the apical turn exhibited a 40 to 60% decrease of the normalized MFI at all ages, when compared to basal turn ($p < 0.001$ for 6 W and 10 W; and $p < 0.010$ for 8 W; one-way ANOVA, post hoc Tukey test). Besides, at 10 W, a significant decrease of fluorescence (about 20%) was observed for middle turn compared to the basal one ($p < 0.050$, one-way ANOVA, post hoc Tukey test) and this KCNQ4 channel expression gradient remains similar as mice grew old (not shown). (n = 3 cochleae from different mice, at least 60 cells were counted at each turn).

DISCUSSION

We investigated the cellular basis of a DFNA2-like hearing loss by analyzing the cochlear cell survival using the C3H/HeJ mouse strain which carries the *Kcnq4* KO allele. Human DFNA2 is generated by the incorporation of at least one subunit carrying a dominant negative mutation in the tetrameric channel complex generated by the heterozygous *KCNQ4*

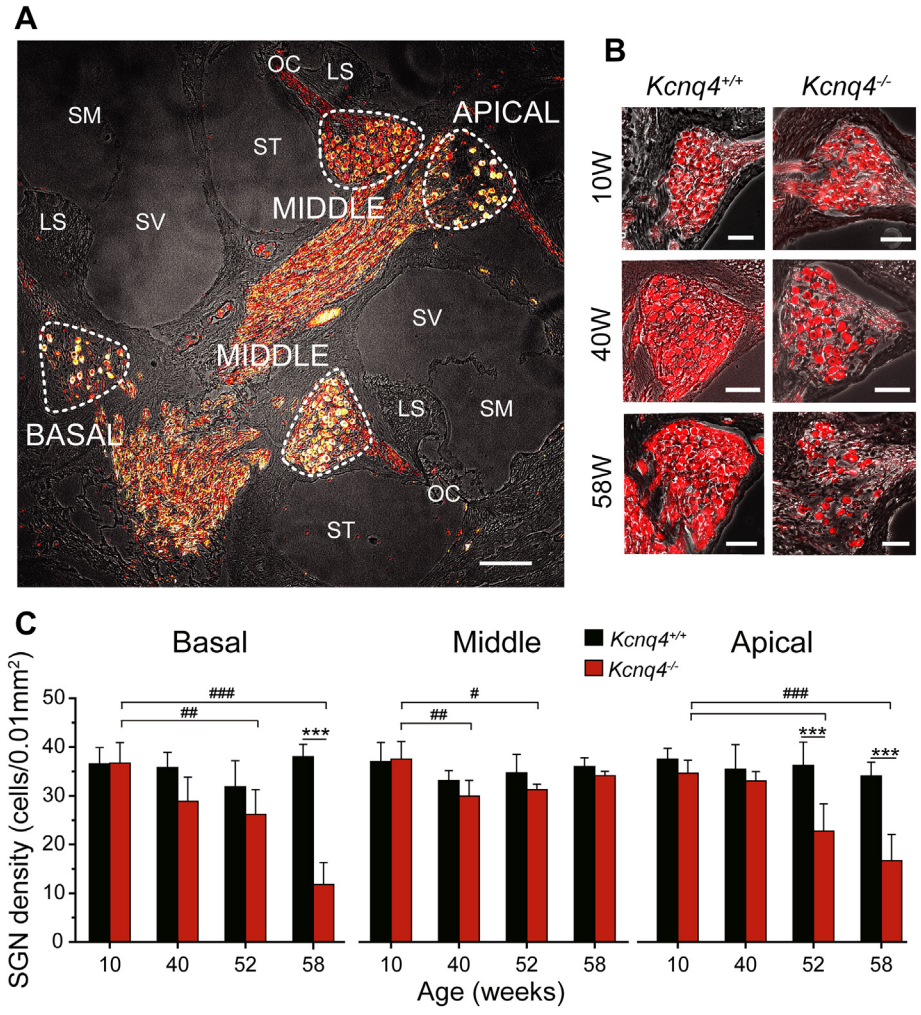

Fig. 6. Spiral ganglion neuron loss in *Kcnq4*$^{-/-}$ mice. (A) Representative picture of a modiolar cochlear section showing cochlear structures including the three turns of the spiral ganglion. The picture was taken from a 52 W *Kcnq4*$^{-/-}$ mice. Neurons were labeled with anti-β-III tubulin (red). White dashed lines delimit spiral ganglia areas. β-III tubulin signal was superimposed on the corresponding light transmission phase contrast pictures. Abbreviations are: SV: Scala vestibuli, SM: Scala media, ST: Scala timpani, OC: Organ of Corti, LS: Limbus spiralis. Cochlear turns are also indicated Scale bar: 100 μm. **(B)** Representative pictures showing SGNs in basal turn from *Kcnq4*$^{+/+}$ and *Kcnq4*$^{-/-}$ mice at 10 W, 40 W and 58 W. β-III tubulin-positive neurons are red-colored. Corresponding phase-contrast pictures are also shown. Scale bar: 50 μm. **(C)** SGN density plots for *Kcnq4*$^{+/+}$ and *Kcnq4*$^{-/-}$ mice through age in basal (left), middle (middle) and apical (right) cochlear turns. SGN density values were obtained counting the number of β-III tubulin-positive neurons in the selected area in each cochlear turn at the indicated age. Data are represented as means ± SEM from three to five independent experiments. Asterisk symbol indicates statistical differences between *Kcnq4*$^{+/+}$ and *Kcnq4*$^{-/-}$ animals at each age and hash symbol indicates statistical differences among ages for *Kcnq4*$^{-/-}$ animals. $p < 0.050$ (#), $p < 0.010$ (##) and $p < 0.001$ (***, ###). Two-way ANOVA, post hoc Bonferroni test.

allele expression. It exhibits a mild to moderate hearing loss during the initial phase that correlates with misfunction of OHCs, evolving to profound hearing loss in its last phase by still unknown mechanisms. In the heterozygous KI mouse model, $I_{K,n}$ current is severely reduced. However, HL develops much slower than homozygous KO mice. Neither heterozygous KI nor homozygous KO mice resembled the last phase of DFNA2 when using a mixed background (Kharkovets et al., 2006). However, expressing the KO allele in the C3H/HeJ inbred mouse strain, we were able to gather many more features that would contribute to explain the cellular alterations displayed in the last phase of DFNA2. For our study, we preferred to use the homozygous KO instead of the heterozygous KI mice (that truly reproduce DFNA2) since the hearing loss develops much faster in the first one (starting ~30 weeks earlier). In fact, the heterozygous KI mouse would have yielded similar results only after 18 months of age. Genetic background is very important for phenotype expressivity which can be modulated by modifier genes, increasing or decreasing it (Doetschman, 2009). Inbred strains have a better control of these genes, but they must be selected carefully. C57BL/6, a very common inbred strain, is a model for ARHL which develops IHC and OHC loss with age (Kane et al., 2012). The C3H/HeJ mouse background offers advantages for our studies of DFNA2 expressivity over other strains because cell survival is very high, even at advanced ages, keeping age-related hair cell death to a minimum (Trune et al., 1996).

Time pattern of OHC, IHC and SGN degeneration in the DFNA2-like mouse model

Previous analysis of the KCNQ4 KO mouse phenotype showed misfunction and degeneration only of OHCs, related to the first phase of DFNA2 hearing loss (Kharkovets et al., 2006). In our current study, besides OHC degeneration, we also established the loss of IHCs and SGNs in the mouse lacking KCNQ4 channel expression. However, these cells die much later than OHCs. In our experiments, we detected a significant IHC death by week 40 that was restricted to the basal turn. The proportion of cell loss is very high in basal regions with a complete absence of IHCs at the hook after 40 W. Additionally, 1-year-old mice had a slight but significant decrease in cell survival in the most apical segments (around 30%). Thus, these data suggest that middle-aged adult KO mice in the C3H/HeJ strain, will undergo a deep HL to high-frequency sounds. This finding may be linked to profound deafness observed in aged DFNA2 patients (De Leenheer et al., 2002; Dominguez and

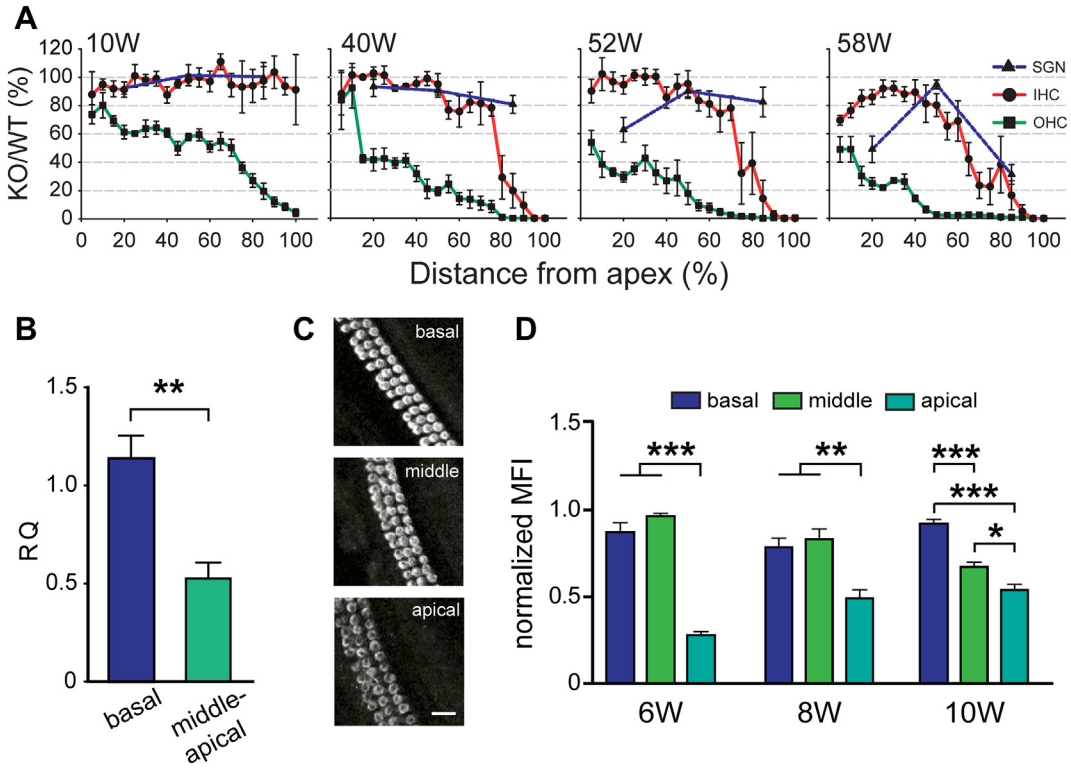

Fig. 7. Spatiotemporal correlation between cell loss and KCNQ4 channel expression. (A) Decrease of OHC (square), IHC (circle) and SGN (triangle) survival from 10 W to 58 W mice. Normalized cell survival was expressed as the ratio between cell counts for *Kcnq4*$^{-/-}$ and *Kcnq4*$^{+/+}$ mice (KO/WT). Data were calculated from cytocochleograms for OHCs and IHCs and neuronal densities for each cochlear turn for SGNs. **(B)** *Kcnq4* gene expression in WT mouse cochleae. Relative quantification (RQ) of *Kcnq4* mRNA was performed in the basal and middle/apical turns of 3 W WT mouse cochleae. Total RNA was extracted and RT-qPCR was performed. The fold change of *Kcnq4* was calculated using $2^{-\Delta\Delta CT}$ and mRNA expression was referred to the geometric mean of the reference genes *Gapdh* and *Hprt*. The basal turn was used as the calibrator. Data are represented as means ± SEM (n = 3 independent experiments, pooling cochleae from three to four animals each time). $p < 0.010$ (**), Student's t-test. **(C)** Representative pictures showing KCNQ4 immunolabeled OHCs in the three different cochlear turns at 10 W mice. Cochlear whole-mounts were processed separately for basal, middle and apical turns. Scale bar, 15 μm. **(D)** Mean fluorescence intensity (MFI) quantification of KCNQ4-positive cells in young adult mice. MFIs were analyzed with Image J software and values were normalized to their maximum at each age, which was considered as the reference fluorescence signal. Data are represented as means ± SEM (n = 3 independent experiment). For each cochlea, we measured at least 60 OHCs in the central region of each turn. At 6 W, ANOVA shows statistically significant differences between apical to basal and middle turns ($p < 0.001$) (***). At 8 W, ANOVA shows statistical differences between apical to basal and middle turns ($p < 0.010$) (**). For 10 W, ANOVA shows statistical differences between apical to basal ($p < 0.001$) (***), between apical to middle ($p < 0.050$) (*) and between middle to basal turns ($p < 0.001$) (***). One-way ANOVA, post hoc Tukey test.

Dodson, 2012). We also found loss of SGNs, starting in middle-aged adults, mostly in parallel with IHC loss. It progresses with age in basal turns, but also in the most apical segments. Distinctly, neuron degeneration was not present in middle turns up to 58 W mice. Although the analysis for SGNs was not so detailed due to technical limitations, we detected a strong reduction in the overall number of neurons. Neuronal loss in apical and basal turns mostly parallels that of IHC, suggesting a link between them. Although cell degeneration is caused by the absence of the KCNQ4 channel, cellular death cannot be totally attributed to its lack.

DFNA2 hearing loss and KCNQ4 channel expression

Cochlear expression of KCNQ4 protein in C3H/HeJ WT mice was detected only in OHCs with a decreasing gradient of channel expression from basal to apical turns in young and adult mice, in accordance with others (Mammano and Ashmore, 1996; Ruttiger et al., 2004; Kharkovets et al., 2006; Winter et al., 2006; Mustapha et al., 2009; Jaumann et al., 2012; Takahashi et al., 2018). The expression gradient is correlated with the progression of OHC death in *Kcnq4*$^{-/-}$ mice obtained in our experiments. This result can be associated with the initial reduction of hearing sensitivity (<60 dB) at high frequencies, which progresses to middle and low frequencies with age in DFNA2 patients (Dominguez and Dodson, 2012). Also, ototoxic drugs that alter KCNQ4 channel function exhibit a similar degenerative profile, where OHCs from basal turns are more sensitive to their deleterious effects (Fausti et al., 1984; Leitner et al., 2011; Sheppard et al., 2015). However, this expression pattern differs from that reported by others. Beisel et al. (Beisel et al., 2005) found that KCNQ4 is highly expressed in OHCs from the apical turn, decreasing towards the basal hook. They also detected the expression of KCNQ4 in IHCs and SGNs, which was higher in basal than apical turns. In contrast, our IF experiments showed KCNQ4 expression neither in IHCs nor in SGNs. The reason for these differences is not clear and could be attributed to the genetic backgrounds employed in each case. Although we could not detect expression of KCNQ4 in IHCs probably by being below the detection limit of the method, several other experimental approaches suggest its presence in this cell type (Marcotti et al., 2003; Oliver et al., 2003; Kharkovets et al., 2006). Channel expression seems to be restricted to the neck of the IHC, along with

the BK channel (Oliver et al., 2003). KCNQ4 is responsible for the $I_{K,n}$ current of IHCs (Kharkovets et al., 2006) which contributes to restore membrane potential (Marcotti et al., 2003; Oliver et al., 2003).

Our results indicate that KCNQ4 plays different roles in cell survival: in OHCs, it contributes to short-to middle-term survival while in IHCs, it participates in long-term survival. In OHCs it is the main potassium extruder while in IHCs it participates in restoring membrane potential (Oliver et al., 2003, Kharkovets et al., 2006). In the first case, its absence generates a 15-mV depolarization. On the other hand, KCNQ4 absence in IHCs slightly depolarizes them (3–5 mV), generating a long-term cumulative deleterious effect, leading to cell death 30 weeks later than OHCs in our model.

The expression of the KCNQ4 channel in SGNs is contradictory. Although we did not find it by immunofluorescence, its expression had been reported by others (Beisel et al., 2005). These neurons exhibit an M-current generated by KCNQ channels (Lv et al., 2010). KCNQ2 and KCNQ3 subunits were reported in SGNs (Jin et al., 2009). Then, the molecular composition of the M-current detected in these studies cannot be ascribed to the KCNQ4 channel and we cannot assert the possibility that cell death could be due to the lack of this channel. It is still unknown whether neuronal degeneration in KO mouse occurs as a primary event due to KCNQ4 absence or if it is a consequence of IHC loss. There is evidence indicating that SGN survival depends on trophic support provided by IHCs (Gillespie and Shepherd, 2005) and supporting cells (Stankovic et al., 2004; Sugawara et al., 2005; Sugawara et al., 2007). The temporal correlation observed between IHC and SGN death links their degenerative process, at least in apical and basal turns. As synaptic disconnection of SGNs has been postulated as an earlier event triggering neuron degeneration (Liberman, 2017), the loss of IHCs observed in adult mice would impact on neuron survival. In summary, SGN death is a later event in the mouse lacking KCNQ4 expression and its cause cannot be certainly attributed to this channel function, but probably to IHC disappearance.

HC death kinetics and neuronal loss significance to DFNA2

The loss of OHCs has been reported previously, but the process is not fully understood (Kharkovets et al., 2006; Dominguez and Dodson, 2012). For this reason, we thoroughly tracked down the cell death kinetics for both hair cell types. To do so, we constructed cytocochleograms for OHC and IHC survival at different ages. This tool enables not only cell count normalization throughout all studied ages but also to compare HL among species (e.g. humans) (Viberg and Canlon, 2004). For OHCs, our spatiotemporal analysis revealed that all segments develop cell degeneration, although at different rates. Surprisingly by week 3, basal segments already showed a pronounced cell loss. As this was the youngest age tested, we assume OHC degeneration had already begun, considering that the KCNQ4 channel is not required for cell differentiation or maturation (Bulankina and Moser, 2012). Cell survival was monitored during several weeks in young and middle-aged animals allowing us to determine cell death rates for each segment. We observed that the basal turn had the highest degeneration rate while for the apical turn was the opposite. When we plotted cell survival for each segment as a function of age, we observed that cell loss was not linear in any cochlear segment. Considering that OHCs from KO and KI mouse models for KCNQ4 are chronically depolarized (Kharkovets et al., 2006), our results suggest that at the initial steps of hearing loss, OHCs are able to endure the altered resting membrane potential for some weeks before starting to die abruptly. Interestingly, the rates for cell death are not uniform. To describe cell death rates we fitted our data with a sigmoidal equation. Kinetic parameters indicated that cell loss in the basal turns occurs faster than in the apical turns. Our data are in agreement with the differential rates observed in DFNA2 patients where hearing loss is faster for high- than for low-frequency sounds (Dominguez and Dodson, 2012). Although the progression of OHC loss in KO mouse is much faster than that observed in heterozygous KI mouse (Kharkovets et al., 2006), our results support this pattern of tissue degeneration. Then, our data indicate that the expression level of KCNQ4 is relevant to the potassium extrusion function in OHCs since there is a direct correlation between channel expression levels and cell death kinetics.

On the other hand, in middle-aged mice, IHC loss follows a different pattern compared to OHCs exhibiting a drastic reduction in cell number. For example, it takes fewer segments to obtain a high percentage of cell loss for IHC than for OHCs. For this reason, we could only analyze the kinetics of cell loss for segments greater than S55. The loss of IHC was not previously reported in other *Kcnq4* transgenic models. However, it has been suggested that IHCs are involved in the process of profound hearing loss reported in aged DFNA2 patients (Dominguez and Dodson, 2012). Our findings show, for the first time, that these cells participate in the progression of deafness since their absence increase hearing threshold more than 70 dB (Willott, 2001). According to our results, this process starts at basal segments, where high-frequency sounds are detected, progressing to middle segments with age, similar to that observed for DFNA2. Surprisingly, older animals (> 1-year-old), also showed IHC degeneration in apical regions, that would impair hearing sensitivity for low-frequency sounds. The heterozygous KI mouse retains 1/16 of the $I_{K,n}$ current, a condition that should occur in DFNA2 patients. The first phase of the disease starts at ~ 15-year-old, while the second phase appears after 65-year-old. The degenerative process is much faster in KO than in KI mice, advancing OHC disappearance (Kharkovets et al., 2006). Therefore, as our model completely lacks the $I_{K,n}$ current, a shift in the life period where HC degeneration occurs, is expected.

Surprisingly we found degeneration of SGNs in basal and apical turns of mice older than 1 year. The participation of SGNs in DFNA2 progression has not been reported. Probably, SGN death is secondary to IHC loss, but its death suggests a progression of neuron degeneration to the CNS, which could affect sound interpretation.

Tissular and structural alterations of OHCs

We determined a differential OHC row degeneration with age. Although most OHCs die, the middle row showed a significantly higher sensitivity to KCNQ4 absence. The contribution of individual OHC rows to hearing has not been clearly established yet. Modeling predictions indicate that hearing amplification requires proper integrity of all three rows of OHCs. However, a controlled exposure to styrene which produces a specific loss of the outer row had no significant effect on cochlear sensitivity (Chen et al., 2008; Murakoshi et al., 2015). Although we have not measured the functional properties of OHCs, we observed alterations in hair bundle structures at early stages that must affect amplificatory function and contribute to hearing impairment before cell death and replacement by supporting cells. Previous reports observed that stereocilia alterations are early events during processes that generate cochlear damage such as NIHL. These correlate with an elevation of the hearing threshold after noise exposure (Slepecky, 1986; Clark and Pickles, 1996; Willott, 2001; Chen et al., 2003; Harrison, 2012). Furthermore, these alterations were also observed in OHCs from a mouse model of ARHL correlated with alterations in otoacoustic emissions (Slepecky, 1986; Le Calvez et al., 1998; Harrison, 2012). These authors reported many of the hair bundle defects shown in our study which include fused, bent, floppy and missing stereocilia. In all these cases, overstimulation of the sensory cells leads to disconnection from the tectorial membrane and crashes between adjacent stereocilia, favoring cell fusion. Loss of rigidity in floppy stereocilia could be generated by actin filament depolymerization and loss of cross-bridges between these filaments (Tilney et al., 1982). Besides, stereocilia disorganization could lead to loss of the tip-links and cross-linkages, which finally would affect the mechanoelectrical transduction of sound waves (Harrison, 2012). In the *Kcnq4* transgenic mice, chronic depolarization of OHCs generated by $I_{K,n}$ current absence or reduction (Kharkovets et al., 2006) would keep mechanical work exerted by prestin constantly active leading to cell overstimulation and damage in a similar fashion to NIHL and ARHL (Chen et al., 2003). The intensity of damage correlates with the amount of remaining $I_{K,n}$ current. Besides, *Kcnq4* gene polymorphisms have been associated with ARHL suggesting that a decrease in KCNQ4 channel function may contribute to its subtle and slow progressive hearing impairment (Van Eyken et al., 2006). Then, the KCNQ4 KO mouse would be a suitable model to investigate in a relative short time period, the molecular mechanisms that lead to audition impairment and to test drugs that may help or prevent several HL pathologies. Sustained depolarization of the cell membrane would pose continuous cellular stress that, depending on its intensity will gate cell death sooner or later. In consequence, a better comprehension of the molecular mechanisms involved in the KCNQ4 channel function would impact in our understanding of these diseases and their treatments.

Our results provide evidence to explain at the cellular level the progression of human DFNA2 from its initial steps to the profound deafness observed in aged patients (i.e. older than 70 years of age). The early stage of HL is compatible with progressive OHC death from basal to apical turns and the later stage correlates with IHC and SGN disappearance. Our data also show that all cells involved in the initial steps of sound transduction are differentially affected by KCNQ4 absence, thus posing the intriguing possibility of a neuronal contribution to the progression of hearing loss.

ACKNOWLEDGMENTS

Our special thanks to Prof. Thomas Jentsch (Max-Delbrück-Centrum für Molekulare Medizin and Leibniz-Institut für Molekulare Pharmakologie, Berlin, Germany) for generously providing *Kcnq4*$^{-/-}$ animals. We also want to thank to Prof. Nélida Winzer for helping us with the statistical analysis. This work was supported by grants from Agencia Nacional de Promoción Científica y Tecnológica (PICT 2016N0260) and Universidad Nacional del Sur (PGI N24/B262) to GS.

CONFLICT OF INTEREST STATEMENT

The authors declare that this work was performed in the absence of conflict of interest.

REFERENCES

Akil O, Lustig LR. (2013) Mouse cochlear whole mount immunofluorescence. In: Bio-protocol 3e332, http://www.bio-protocol.org/e332.

Barclay M, Ryan AF, Housley GD. (2011) Type I vs type II spiral ganglion neurons exhibit differential survival and neuritogenesis during cochlear development. Neural Dev 6:33, https://doi.org/10.1186/1749-8104-6-33.

Beisel KW, Nelson NC, Delimont DC, Fritzsch B. (2000) Longitudinal gradients of KCNQ4 expression in spiral ganglion and cochlear hair cells correlate with progressive hearing loss in DFNA2. Brain Res Mol Brain Res 82:137-149, https://doi.org/10.1016/s0169-328x(00)00204-7.

Beisel KW, Rocha-Sanchez SM, Morris KA, Nie L, Feng F, Kachar B, Yamoah EN, Fritzsch B. (2005) Differential expression of KCNQ4 in inner hair cells and sensory neurons is the basis of progressive high-frequency hearing loss. J Neurosci 25:9285-9293, https://doi.org/10.1523/JNEUROSCI.2110-05.2005.

Boyce RW, Dorph-Petersen KA, Lyck L, Gundersen HJ. (2010) Design-based stereology: introduction to basic concepts and practical approaches for estimation of cell number. Toxicol Pathol 38:1011-1025, https://doi.org/10.1177/0192623310385140.

Bulankina AV, Moser T. (2012) Neural circuit development in the mammalian cochlea. Physiology (Bethesda) 27:100-112, https://doi.org/10.1152/physiol.00036.2011.

Chen YS, Liu TC, Cheng CH, Yeh TH, Lee SY, Hsu CJ. (2003) Changes of hair cell stereocilia and threshold shift after acoustic trauma in guinea pigs: comparison between inner and outer hair cells. ORL; journal for oto-rhino-laryngology and its related specialties, Vol. 65, 2003266-274, https://doi.org/10.1159/000075224.

Chen GD, Tanaka C, Henderson D. (2008) Relation between outer hair cell loss and hearing loss in rats exposed to styrene. Hear Res 243:28-34, https://doi.org/10.1016/j.heares.2008.05.008.

Clark JA, Pickles JO. (1996) The effects of moderate and low levels of acoustic overstimulation on stereocilia and their tip links in the Guinea pig. Hear Res 99:119-128.

Dallos P. (2008) Cochlear amplification, outer hair cells and prestin. Curr Opin Neurobiol 18:370-376, https://doi.org/10.1016/j.conb.2008.08.016.

Davis RR, Newlander JK, Ling X, Cortopassi GA, Krieg EF, Erway LC. (2001) Genetic basis for susceptibility to noise-induced hearing loss in mice. Hear Res 155:82-90.

De Leenheer EM, Ensink RJ, Kunst HP, Marres HA, Talebizadeh Z, Declau F, Smith SD, Usami S, Van de Heyning PH, Van Camp G, Huygen PL, Cremers CW. (2002) DFNA2/KCNQ4 and its

manifestations. Adv Otorhinolaryngol 61:41-46, https://doi.org/10.1159/000066802.
Doetschman T. (2009) Influence of genetic background on genetically engineered mouse phenotypes. Methods Mol Biol 530:423-433, https://doi.org/10.1007/978-1-59745-471-1_23.
Dominguez LM, Dodson KM. (2012) Genetics of hearing loss: focus on DFNA2. The application of clinical genetics 5:97-104, https://doi.org/10.2147/TACG.S35525.
Erway LC, Willott JF, Archer JR, Harrison DE. (1993) Genetics of age-related hearing loss in mice: I. inbred and F1 hybrid strains. Hear Res 65:125-132.
Fausti SA, Rappaport BZ, Schechter MA, Frey RH, Ward TT, Brummett RE. (1984) Detection of aminoglycoside ototoxicity by high-frequency auditory evaluation: selected case studies. Am J Otolaryngol 5:177-182, https://doi.org/10.1016/s0196-0709(84)80009-5.
Fransen E, Lemkens N, Van Laer L, Van Camp G (2003) Age-related hearing impairment (ARHI): environmental risk factors and genetic prospects. Exp Gerontol 38:353–359.https://doi.org/10.1016/s0531-5565(03)00032–9.
Gillespie LN, Shepherd RK. (2005) Clinical application of neurotrophic factors: the potential for primary auditory neuron protection. Eur J Neurosci 22:2123-2133, https://doi.org/10.1111/j.1460-9568.2005.04430.x.
Harrison RV (2012) The prevention of noise induced hearing loss in children. International journal of pediatrics 2012:473541.https://doi.org/10.1155/2012/473541
Hibino H, Kurachi Y. (2006) Molecular and physiological bases of the K^+ circulation in the mammalian inner ear. Physiology 21:336-345, https://doi.org/10.1152/physiol.00023.2006.
Holt JR, Stauffer EA, Abraham D, Géléoc GS. (2007) Dominant-negative inhibition of M-like potassium conductances in hair cells of the mouse inner ear. J Neurosci 27:8940-8951.
Jaumann M, Dettling J, Gubelt M, Zimmermann U, Gerling A, Paquet-Durand F, Feil S, Wolpert S, Franz C, Varakina K, Xiong H, Brandt N, Kuhn S, Geisler HS, Rohbock K, Ruth P, Schlossmann J, Hutter J, Sandner P, Feil R, Engel J, Knipper M, Ruttiger L. (2012) cGMP-Prkg1 signaling and Pde5 inhibition shelter cochlear hair cells and hearing function. Nat Med 18:252-259, https://doi.org/10.1038/nm.2634.
Jin Z, Liang GH, Cooper EC, Jarlebark L. (2009) Expression and localization of K channels KCNQ2 and KCNQ3 in the mammalian cochlea. Audiol Neurootol 14:98-105, https://doi.org/10.1159/000158538.
Kane KL, Longo-Guess CM, Gagnon LH, Ding D, Salvi RJ, Johnson KR. (2012) Genetic background effects on age-related hearing loss associated with Cdh23 variants in mice. Hear Res 283:80-88, https://doi.org/10.1016/j.heares.2011.11.007.
Kharkovets T, Hardelin JP, Safieddine S, Schweizer M, El-Amraoui A, Petit C, Jentsch TJ. (2000) KCNQ4, a K^+-channel mutated in a form of dominant deafness, is expressed in the inner ear and the central auditory pathway. Proc Natl Acad Sci U S A 97:4333-4338, https://doi.org/10.1073/pnas.97.8.4333.
Kharkovets T, Dedek K, Maier H, Schweizer M, Khimich D, Nouvian R, Vardanyan V, Leuwer R, Moser T, Jentsch TJ. (2006) Mice with altered KCNQ4 K^+ channels implicate sensory outer hair cells in human progressive deafness. EMBO J 25:642-652, https://doi.org/10.1038/sj.emboj.7600951.
Kubisch C, Schroeder BC, Friedrich T, Lütjohann B, El-Amraoui A, Marlin S, Petit C, Jentsch TJ. (1999) KCNQ4, a novel potassium channel expressed in sensory outer hair cells, is mutated in dominant deafness. Cell 96:437-446, https://doi.org/10.1016/s0092-8674(00)80556-5.
Kurima K, Ebrahim S, Pan B, Sedlacek M, Sengupta P, Millis BA, Cui R, Nakanishi H, Fujikawa T, Kawashima Y, Choi BY, Monahan K, Holt JR, Griffith AJ, Kachar B. (2015) TMC1 and TMC2 localize at the site of mechanotransduction in mammalian inner ear hair cell stereocilia. Cell Rep 12:1606-1617, https://doi.org/10.1016/j.celrep.2015.07.058.
Lang F, Vallon V, Knipper M, Wangemann P. (2007) Functional significance of channels and transporters expressed in the inner ear and kidney. Am J Physiol Cell Physiol 293:C1187-C1208, https://doi.org/10.1152/ajpcell.00024.2007.
Le Calvez S, Guilhaume A, Romand R, Aran JM, Avan P. (1998) CD1 hearing-impaired mice. II. Group latencies and optimal f2/f1 ratios of distortion product otoacoustic emissions, and scanning electron microscopy. Hear Res 120:51-61.
Leitner MG, Halaszovich CR, Oliver D. (2011) Aminoglycosides inhibit KCNQ4 channels in cochlear outer hair cells via depletion of phosphatidylinositol(4,5)bisphosphate. Mol Pharmacol 79:51-60, https://doi.org/10.1124/mol.110.068130.
Liberman MC. (2017) Noise-induced and age-related hearing loss: new perspectives and potential therapies. F1000Research 6:927, https://doi.org/10.12688/f1000research.11310.1.
Livak KJ, Schmittgen TD. (2001) Analysis of relative gene expression data using real-time quantitative PCR and the 2(−Delta Delta C(T)) method. Methods 25:402-408, https://doi.org/10.1006/meth.2001.1262.
Lv P, Wei D, Yamoah EN. (2010) Kv7-type channel currents in spiral ganglion neurons: involvement in sensorineural hearing loss. J Biol Chem 285:34699-34707, https://doi.org/10.1074/jbc.M110.136192.
Mammano F, Ashmore JF. (1996) Differential expression of outer hair cell potassium currents in the isolated cochlea of the guinea-pig. J Physiol 496:639-646, https://doi.org/10.1113/jphysiol.1996.sp021715 Pt 3.
Marcotti W, Johnson SL, Holley MC, Kros CJ. (2003) Developmental changes in the expression of potassium currents of embryonic, neonatal and mature mouse inner hair cells. J Physiol 548:383-400, https://doi.org/10.1113/jphysiol.2002.034801.
Mistrik P, Ashmore J. (2009) The role of potassium recirculation in cochlear amplification. Curr Opin Otolaryngol Head Neck Surg 17:394-399, https://doi.org/10.1097/MOO.0b013e328330366f.
Montgomery SC, Cox BC. (2016) Whole mount dissection and immunofluorescence of the adult mouse cochlea. J Vis Exp , https://doi.org/10.3791/53561.
Muller M, von Hunerbein K, Hoidis S, Smolders JW. (2005) A physiological place-frequency map of the cochlea in the CBA/J mouse. Hear Res 202:63-73, https://doi.org/10.1016/j.heares.2004.08.011.
Murakoshi M, Suzuki S, Wada H. (2015) All three rows of outer hair cells are required for cochlear amplification. Biomed Res Int 2015727434, https://doi.org/10.1155/2015/727434.
Mustapha M, Fang Q, Gong TW, Dolan DF, Raphael Y, Camper SA, Duncan RK. (2009) Deafness and permanently reduced potassium channel gene expression and function in hypothyroid Pit1dw mutants. J Neurosci 29:1212-1223, https://doi.org/10.1523/JNEUROSCI.4957-08.2009.
Nie L. (2008) KCNQ4 mutations associated with nonsyndromic progressive sensorineural hearing loss. Curr Opin Otolaryngol Head Neck Surg 16:441-444, https://doi.org/10.1097/moo.0b013e32830f4aa3.
Oliver D, Knipper M, Derst C, Fakler B. (2003) Resting potential and submembrane calcium concentration of inner hair cells in the isolated mouse cochlea are set by KCNQ-type potassium channels. J Neurosci 23:2141-2149, https://doi.org/10.1523/jneurosci.23-06-02141.2003.
Pan B, Akyuz N, Liu XP, Asai Y, Nist-Lund C, Kurima K, Derfler BH, Gyorgy B, Limapichat W, Walujkar S, Wimalasena LN, Sotomayor M, Corey DP, Holt JR. (2018) TMC1 forms the pore of mechanosensory transduction channels in vertebrate inner ear hair cells. Neuron 99:736-753 e736, https://doi.org/10.1016/j.neuron.2018.07.033.
Ruttiger L, Sausbier M, Zimmermann U, Winter H, Braig C, Engel J, Knirsch M, Arntz C, Langer P, Hirt B, Muller M, Kopschall I, Pfister M, Munkner S, Rohbock K, Pfaff I, Rusch A, Ruth P, Knipper M. (2004) Deletion of the Ca^{2+}-activated potassium (BK) α-subunit but not the BKβ1-subunit leads to progressive hearing loss. Proc Natl Acad Sci U S A 101:12922-12927, https://doi.org/10.1073/pnas.0402660101.
Sanz L, Murillo-Cuesta S, Cobo P, Cediel-Algovia R, Contreras J, Rivera T, Varela-Nieto I, Avendano C. (2015) Swept-sine noise-induced damage as a hearing loss model for preclinical assays. Front Aging Neurosci 7:7, https://doi.org/10.3389/fnagi.2015.00007.
Sheppard AM, Chen GD, Salvi R. (2015) Potassium ion channel openers, Maxipost and Retigabine, protect against peripheral salicylate ototoxicity in rats. Hear Res 327:1-8, https://doi.org/10.1016/j.heares.2015.04.007.

Slepecky N. (1986) Overview of mechanical damage to the inner ear: noise as a tool to probe cochlear function. Hear Res 22:307-321, https://doi.org/10.1016/0378-5955(86)90107-3.

Spitzmaul G, Tolosa L, Winkelman BH, Heidenreich M, Frens MA, Chabbert C, de Zeeuw CI, Jentsch TJ. (2013) Vestibular role of KCNQ4 and KCNQ5 K^+ channels revealed by mouse models. J Biol Chem 288:9334-9344, https://doi.org/10.1074/jbc.m112.433383.

Stankovic K, Rio C, Xia A, Sugawara M, Adams JC, Liberman MC, Corfas G. (2004) Survival of adult spiral ganglion neurons requires erbB receptor signaling in the inner ear. J Neurosci 24:8651-8661, https://doi.org/10.1523/JNEUROSCI.0733-04.2004.

Sugawara M, Corfas G, Liberman MC. (2005) Influence of supporting cells on neuronal degeneration after hair cell loss. Journal of the Association for Research in Otolaryngology : JARO 6:136-147, https://doi.org/10.1007/s10162-004-5050-1.

Sugawara M, Murtie JC, Stankovic KM, Liberman MC, Corfas G. (2007) Dynamic patterns of neurotrophin 3 expression in the postnatal mouse inner ear. J Comp Neurol 501:30-37, https://doi.org/10.1002/cne.21227.

Takahashi S, Sun W, Zhou Y, Homma K, Kachar B, Cheatham MA, Zheng J. (2018) Prestin contributes to membrane compartmentalization and is required for normal innervation of outer hair cells. Front Cell Neurosci 12:211, https://doi.org/10.3389/fncel.2018.00211.

Tilney LG, Saunders JC, Egelman E, DeRosier DJ. (1982) Changes in the organization of actin filaments in the stereocilia of noise-damaged lizard cochleae. Hear Res 7:181-197.

Trune DR, Kempton JB, Mitchell C. (1996) Auditory function in the C3H/HeJ and C3H/HeSnJ mouse strains. Hear Res 96:41-45, https://doi.org/10.1016/0378-5955(96)00017-2.

Van Eyken E, Van Laer L, Fransen E, Topsakal V, Lemkens N, Laureys W, Nelissen N, Vandevelde A, Wienker T, Van De Heyning P, Van Camp G. (2006) KCNQ4: a gene for age-related hearing impairment? Hum Mutat 27:1007-1016, https://doi.org/10.1002/humu.20375.

Van Laer L, Carlsson PI, Ottschytsch N, Bondeson ML, Konings A, Vandevelde A, Dieltjens N, Fransen E, Snyders D, Borg E, Raes A, Van Camp G. (2006) The contribution of genes involved in potassium-recycling in the inner ear to noise-induced hearing loss. Hum Mutat 27:786-795, https://doi.org/10.1002/humu.20360.

Viberg A, Canlon B. (2004) The guide to plotting a cochleogram. Hear Res 197:1-10, https://doi.org/10.1016/j.heares.2004.04.016.

Vikhe Patil K, Canlon B, Cederroth CR. (2015) High quality RNA extraction of the mammalian cochlea for qRT-PCR and transcriptome analyses. Hear Res 325:42-48, https://doi.org/10.1016/j.heares.2015.03.008.

Willott JF. (2001) Handbook of mouse auditory research: from behavior to molecular biology. CRC Press, 2001.

Winter H, Braig C, Zimmermann U, Geisler HS, Franzer JT, Weber T, Ley M, Engel J, Knirsch M, Bauer K, Christ S, Walsh EJ, McGee J, Kopschall I, Rohbock K, Knipper M. (2006) Thyroid hormone receptors TRalpha1 and TRbeta differentially regulate gene expression of Kcnq4 and prestin during final differentiation of outer hair cells. J Cell Sci 119:2975-2984, https://doi.org/10.1242/jcs.03013.

Wong AC, Ryan AF. (2015) Mechanisms of sensorineural cell damage, death and survival in the cochlea. Front Aging Neurosci 7:58, https://doi.org/10.3389/fnagi.2015.00058.

Zdebik AA, Wangemann P, Jentsch TJ. (2009) Potassium ion movement in the inner ear: insights from genetic disease and mouse models. Physiology 24:307-316, https://doi.org/10.1152/physiol.00018.2009.

(Received 12 December 2018, Accepted 7 May 2019)
(Available online 16 May 2019)